Available online at www.sciencedirect.com
ScienceDirect
Journal of Power Sources 161 (2006) 143–159
JOURNAL OF POWER SOURCES
www.elsevier.com/locate/jpowsour

Water and thermal management in a single PEM fuel cell with non-uniform stack temperature

Yi Zong, Biao Zhou *, Andrzej Sobiesiak

Department of Mechanical, Automotive and Materials Engineering, University of Windsor, Ont., Canada N9B 3P4

Received 16 December 2005; received in revised form 5 February 2006; accepted 6 February 2006
Available online 9 June 2006

Abstract

A non-isothermal, non-isobaric water and thermal management model with phase change has been developed to simulate the mass and energy (sensible heat, latent heat, chemical reaction energy, electrical energy) transfer processes inside a PEM fuel cell unit with a non-uniform stack temperature (hereafter the stack temperature has the same meaning of the cell temperature since only single cell is considered). Based on this model, the following parameters can be predicted along the channels on both cathode and anode sides: current density, output voltage, stack temperature, stream pressure and temperatures, stream velocity, relative humidity, water vapor mole fraction, water liquid fraction, density, viscosity, Reynolds number, required pumping power, and so on. Also, the results from uniform stack temperature model and non-uniform stack temperature model are compared in this research.

Keywords: PEM fuel cell; Water; Thermal management; Mathematical model; Humidification; Pressure drop

1. Introduction

Most current automobiles are driven by internal combustion engines which consume fossil fuel and generate air pollution. With the increasing public concerns of environmental protection, it is predictable that more and more strict regulations will be enforced to reduce or limit the emission of these vehicles in the future. For example, California's zero emission vehicle (ZEV) mandate [1] requires 10% of the vehicles sold by the automotive manufacturers after year 2004 to be ZEVs [2]. Similarly, European auto-companies are required to meet their voluntary carbon dioxide (CO_2) emission limits set by the European Union [3]. According to the Kyoto Protocol, the international community is committed to cut greenhouse gas emissions step by step. The CO_2 emitted by automobiles is one of the major components of greenhouse effects. World Governments, including the Canadian Government, have already invested a lot in exploring new ways to replace the internal combustion engine in automobiles. Among all the technical proposals, the fuel cell is one of the most potential and feasible solutions to achieve this goal. The benefits of using fuel cells are as follows [4]: firstly, fuel cells consume hydrogen instead of the exhaustible fossil fuel, which eventually protect our natural resource and environment; secondly, fuel cells emit only water, therefore, there is no pollution at all. Among all the currently existing fuel cells, the proton exchange membrane (PEM) fuel cell has been widely considered as one of the most promising candidates for automobiles since it has one additional advantage over many other fuel cells; the PEM can operate at room temperature for quick startup.

In recent years, many computer models of PEM fuel cell have been developed. Fuller and Newman [5] developed a non-isothermal model by including the material balances in the channel, the concentration and temperature gradients along the channel as well as across the membrane surface. Nguyen and White [6] studied the variation in current density, water transport, and flow temperatures along the channel. They also modeled the effect of varying anode inlet humidity. Subsequently, an advanced model was developed by Yi and Nguyen [7] to compare different fuel cell designs with coflow and counterflow heat exchangers. In this analysis, they include the thermal mass of the stack, account for the impact of the pressure difference between anode and cathode on water transport in the cell. However, a clear validation of results in both of the analyses was not presented. Mosdale and Srinivasan [8] gave a good review

* Corresponding author. Tel.: +1 519 253 3000x2630; fax: +1 519 973 7007.
E-mail address: bzhou@uwindsor.ca (B. Zhou).

0378-7753/$ – see front matter © 2006 Elsevier B.V. All rights reserved.
doi:10.1016/j.jpowsour.2006.02.107

Nomenclature

a	water vapor activity in stream
A_c	the heat transfer area between stack and flow in a control volume (cm^2)
A_{cool}	the heat transfer area between stack and coolant (cm^2)
A_{cross}	the cross-section area of channel (cm^2)
A_s	the cross-section area of stack (cm^2)
C_{MW}	concentration of water at interface of the membrane ($mol\,cm^{-3}$)
$C_{p,i}$	heat capacity of species i ($J\,mol^{-1}\,K^{-1}$)
d	channel height (cm)
dp	pressure drop (Pa)
D	hydraulic diameter of channel (cm)
D_w	diffusion coefficient of water ($cm^2\,s^{-1}$)
D^0	parameter used in expression for diffusion coefficient of water ($cm^2\,s^{-1}$)
$f(x)$	friction factor
F	Faraday constant, 96,487 C equiv.$^{-1}$
h	channel width (cm)
I	current (A)
$I(x)$	current density ($A\,cm^{-2}$)
I^0	exchange current density for the oxygen reaction ($A\,cm^{-2}$)
k	thermal conductivity of the stream ($W\,m^{-1}\,{}^\circ C^{-1}$)
k_c	evaporation and condensation rate constant (s^{-1})
L	length of channel (cm)
M	equivalent weight of a dry membrane ($g\,mol^{-1}$)
M_i	molecular weight of species i ($g\,mol^{-1}$)
n_d	electro-osmotic drag coefficient (number of water molecules carried by per proton)
N	mole number of species in the stream ($mol\,s^{-1}$)
N_{ch}	number of channel (s)
NE	number of electrons ($A^{-1}\,s^{-1}$)
p_i	partial pressure of species i (Pa)
P	cell total pressure (Pa)
P_{pump}	pumping power (W)
q	energy ($J\,s^{-1}$)
Q	volume flowrate ($m^3\,s^{-1}$)
R_u	the ideal-gas constant ($8.3144\,J\,mol^{-1}\,K^{-1}$)
Re	Reynolds number
RH	relative humidity
S	entropy ($J\,mol^{-1}\,K^{-1}$)
t	thickness (cm)
T	temperature of stream (K)
T_s	temperature of stack (K)
U	overall heat transfer coefficient ($J\,s^{-1}\,cm^{-2}\,{}^\circ C^{-1}$)
V	flow velocity ($m\,s^{-1}$)
V_{cell}	cell voltage (V)
x	direction along the channel length
y	direction normal to the channel length

Greek letters

α	excess coefficients of air (oxygen)
α_{area}	reaction area coefficient
β_{H_2}	mole fraction of hydrogen (100%)
β_{O_2}	mole fraction of oxygen in air (20.9%)
ϕ	water content in stream
η	overpotential for the oxygen reaction (V)
μ	dynamic viscosity ($N\,s\,m^{-2}$)
ρ	density ($kg\,m^{-3}$)
$\rho_{m,dry}$	density of a dry membrane ($g\,cm^{-3}$)
σ_m	membrane conductivity ($\Omega^{-1}\,cm^{-1}$)

Subscripts

air	dry air
avg	average
A	anode
cell	the unit fuel cell
concentration	the concentration of species in the streams
cool	cooling system
C	cathode
drag	electro-osmotic drag
e	electron
ele	electricity
gas	species except water vapor and water liquid
gen	generated
heat	heat
H_2	hydrogen
H_2O	produced water
in	inlet of channel
latent	latent heat
liquid	liquid water in the flow
loss	energy released to environment
m	membrane
MW	water in membrane
N_2	nitrogen
oc	open circuit
O_2	oxygen
pressure	the partial pressure in the streams
pump	the pump supplied the reactants to fuel cell
room	environment
rxn	reaction
sat	saturation
sen	sensible
stack	the stack of fuel cell
system	a closed system
vapor	water vapor in the flow
water	all water including vapor and liquid in the flow
0	in the standard state
1 A	per ampere
#	cathode or anode

on the work that has been conducted at Texas A&M University. In this review, various models are compared and the effect of different humidification on the performance of the fuel cell is discussed. Unfortunately, this paper does not give the exact details of their modeling approaches. Amphlett et al. [9,10] have developed PEM fuel cell models that are based on both the theoretical mechanistic analysis and empirical data. They perform an empirical treatment of the membrane and explain the water transport processes in the membrane. Nevertheless, this model cannot predict some parameters, such as anode humidification, temperature, pressure and so on. Researchers such as Marr and Li [11], Dannenberg et al. [12], Hertwig et al. [13], Ge and Yi [14] and Xue et al. [15] have been performing fuel cell modeling for many years and have made very impressive progress. Those models emphasized important characteristics of the membrane, electrodes, as well as a detailed description of the water content in the membrane. In order to simplify the process, most models are isothermal and isobaric and with a uniform stack temperature. These parameters, e.g., stream temperature and pressure, stack temperature are crucial for optimizing PEM fuel cells. However, few papers in the available literature addressed them in detail. Zhou et al. [16] from the same group as the present paper, proposed a non-isothermal and non-isobaric model with phase change effects to address these challenges, although the stack temperature was also assumed to be uniform to simplify the real complex processes inside the PEM fuel cells.

In the present study, the model, proposed by Zhou et al. [16], will be extended to a non-isothermal and non-isobaric model with non-uniform stack temperature. This improved model and some simulation results are presented below.

2. Mathematical model

Fig. 1 shows a typical construction of a PEM fuel cell. In the present study, two coordinate axes are chosen. The *x*-axis is along to the gas channels. The temperature, pressure and concentration of gas flow will be calculated along this direction. The *y*-axis is perpendicular to the membrane. The hydrogen ions and water molecules transport from anode to cathode along this direction.

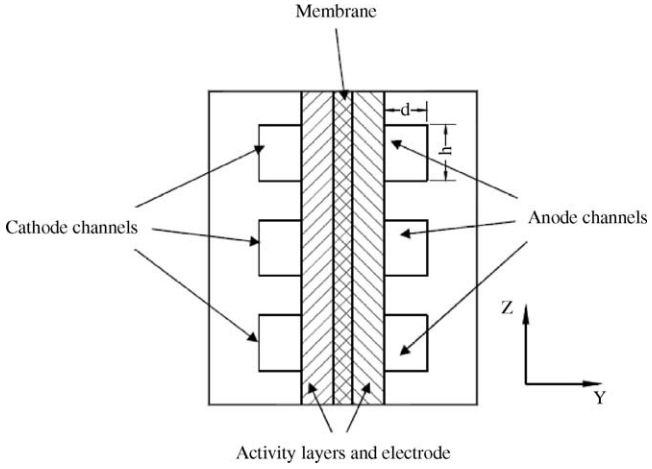

Fig. 1. Schematic diagram of PEM fuel cell modeling regions.

The model includes the following parts: mass balance, energy balance, pressure drop and cell output voltage.

Although most of the equations have been presented in Zhou et al. [16], they are repeated here for completeness.

2.1. Basic assumptions

In the present model, the water transport mechanisms in the membrane are based on the study by Yi and Nguyen's study [7]. Some corresponding assumptions are listed as follows:

1. Only water vapor can diffuse into the electrode and pass through the membrane.
2. The electrode layer is "ultra thin", gas diffusion through the electrode porous layer is neglected.
3. The gases and water vapor are fully mixed, and the mixture is ideal gas.
4. Liquid water exists only in the form of small droplets and the volume is negligible.
5. Water vapor is produced in the electrochemical reaction. This assumption could bring some inaccuracy since the operating temperature is usually under 100 °C. In reality, the product water could be liquid water, or part of water vapor and part of liquid water depending on the local conditions.
6. No voltage drop exists along the flow channels. This assumption was made to simplify the real situation. It is a reasonable assumption because the bipolar plate, usually made from graphite, has a high electrical conductivity.
7. The channels in each unit cell have the same geometry and same surface roughness.
8. A single channel is assumed to represent the unit cell for numerical simulations.
9. The temperature of the solid (including MEA and plates) is assumed to be constant in the *y*-direction only.

2.2. Mass balance

Fig. 2 shows the mass balance in a unit fuel cell. The amount of inlet gases is calculated according to the amount of gases consumed by the electrochemical reaction for PEM fuel cell: $2H_2 + O_2 = 2H_2O$. One equivalence of electrons is 1 mole of electrons or 6.022×10^{23} electrons (Avagadro's number). This quantity of electrons has the charge of 96,487 coulombs (C) (Faraday's Constant). Therefore, the charge of a single electron

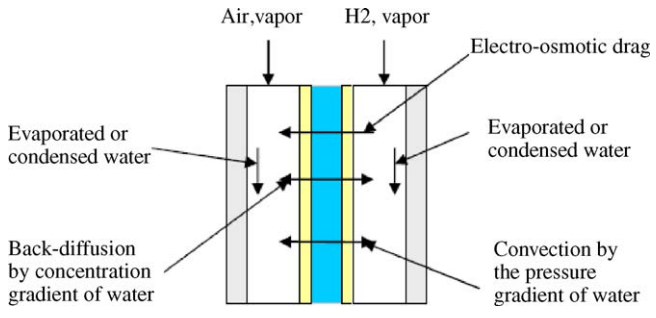

Fig. 2. Mass balance of a unit fuel cell.

is 1.602×10^{-19} C. One ampere of current is defined as 1 C s^{-1}. As a result, the mole number of electrons for 1 A of current is as follows:

$$n_e = \frac{NE_{1\,A}}{6.022 \times 10^{23}} = 1.03656546 \times 10^{-5}\ \text{mole}\,(\text{A s})^{-1} \quad (1)$$

where $NE_{1\,A}$ represents the number of electrons of 1 A. It can be calculated by $NE_{1\,A} = 1/1.602 \times 10^{-19}$. Based on the reaction equation, the theoretical mole numbers of consumed oxygen and hydrogen, and produced water for 1 A current output can be obtained by the following equations:

$$n_{O_2,1\,A} = \tfrac{1}{4} n_e \quad (2)$$

$$n_{H_2O,1\,A} = \tfrac{2}{4} n_e = \tfrac{1}{2} n_e \quad (3)$$

$$n_{H_2,1\,A} = \tfrac{2}{4} n_e = \tfrac{1}{2} n_e \quad (4)$$

The excess coefficients for air (oxygen) or hydrogen is defined as

$$\alpha = \frac{\text{actually supplied mole number of air (oxygen) or hydrogen}}{\text{theoretically consumed mole number of air (oxygen) or hydrogen}} \quad (5)$$

Therefore, the supplied oxygen, nitrogen and hydrogen mole numbers can be calculated by the following equations:

$$n_{O_2,in,1\,A} = \alpha_{O_2} n_{O_2,1\,A} \quad (6)$$

$$n_{N_2,in,1\,A} = n_{O_2,in,1\,A} \frac{1 - \beta_{O_2}}{\beta_{O_2}} \quad (7)$$

$$n_{H_2,in,1\,A} = \frac{\alpha_{H_2} n_{H_2,1\,A}}{\beta_{H_2}} \quad (8)$$

where β_{O_2} is the mole fraction of oxygen in air ($\beta_{O_2} = 20.9\%$) and β_{H_2} is that of the hydrogen in anode ($\beta_{H_2} = 1$ in the present study).

For generating I amperes of current, the molar flowrates of oxygen, nitrogen and hydrogen for the single channel are evaluated in (mol s^{-1}) as

$$N_{C,O_2,in} = \frac{I n_{O_2,in,1\,A}}{N_{ch}} \quad (9)$$

$$N_{C,N_2,in} = N_{C,O_2,in} \frac{1 - \beta_{O_2}}{\beta_{O_2}} \quad (10)$$

$$N_{A,H_2,in} = I \frac{n_{H_2,in,1\,A}}{N_{ch}} \quad (11)$$

The components of the mixture vary along the channels and the local molar flowrates in channel are defined as follows:

$$\frac{dN_{C,O_2}(x)}{dx} = -n_{O_2,1\,A} I(x) h \alpha_{area} \quad (12)$$

$$\frac{dN_{C,N_2}(x)}{dx} = 0 \quad (13)$$

$$\frac{dN_{A,H_2}(x)}{dx} = -n_{H_2,1\,A} I(x) h \alpha_{area} \quad (14)$$

where α_{area} is the reaction area coefficient that accounts for the land area for reaction due to gas diffusion from the channel to diffusion layer.

The variations of vapor and liquid water along the channels are more complicated. Water vapor transport and condensation, and liquid water evaporation are considered in this model. There are three water transport mechanisms across the membrane, according Yi and Nguyen [7]: (a) electro-osmotic drag—since the hydrogen ions pass through the membrane, the water molecules are carried from the anode to the cathode; (b) back-diffusion by the concentration gradient of water—because the water concentration is different, some water molecules diffuse from the cathode to the anode; (c) convection by the pressure gradient—water moves from higher-pressure side to the lower one. In a calculated volume, usually it is very small if the grid size is small enough, there is negligible potential gradient in the x-direction within the calculated volume. The electro-osmotic drag flux (mol s^{-1}) in the y-direction is as follows [6]:

$$N_{drag}(y) = \frac{n_d(x) I(x)}{F} \quad (15)$$

where $I(x)$ is the local current density of the fuel cell, F is Faraday's constant, n_d the electro-osmotic drag coefficient which represents the number of water molecules carried by one proton and is calculated by [6]:

$$n_d(x) = \begin{cases} 0.0049 + 2.02a(x) - 4.53a^2(x) + 4.09a^3(x) & 0 < a(x) \le 1 \\ 1.5849 + 0.159(a(x) - 1) & a(x) > 1 \end{cases} \quad (16)$$

where $a(x)$ is the activity of water vapor in membrane. Since the membrane is placed between the cathode and anode, the water vapor activity in the membrane is affected by the water vapor activity at both cathode and anode. A weighted average water activity for the water vapor activity in the membrane is employed. The water vapor activity at anode or cathode $a_\#(x)$ is defined as [6]:

$$a_\#(x) = \frac{N_{\#,vapor}(x)}{\sum_i N_{\#,i}(x)} \frac{p_\#(x)}{p_{\#,sat}(x)} \quad (i, \text{the species in the flow stream \#}) \quad (17)$$

The water vapor activity at the membrane is defined as

$$a_M(x) = \alpha_M a_A(x) + (1 - \alpha_M) a_C(x) \quad (18)$$

where α_M is the weight coefficient. Thus, the water vapor activity at the membrane depends on the water activity at both cathode and anode.

The diffusion flux caused by the concentration gradient of water can be written as follows:

$$N_{concentration}(y) = D_{MW} \left(\frac{\partial c_{MW}}{\partial y} \right) \quad (19)$$

where the diffusion coefficient of water is as follows [7]:

$$D_{\mathrm{MW}} = \begin{cases} (0.0049 + 2.02a(x) - 4.53a^2(x) + 4.09a^3(x))D^0 \exp\left[2416\left(\dfrac{1}{303} - \dfrac{1}{T_\mathrm{s}(x)}\right)\right] & \text{for } 0 < a(x) \le 1 \\ 1.59 + 0.159[(a(x) - 1)]D^0 \exp\left[2416\left(\dfrac{1}{303} - \dfrac{1}{T_\mathrm{s}(x)}\right)\right] & \text{for } a(x) > 1 \end{cases} \tag{20}$$

Convection flux caused by pressure gradient [7] is

$$N_{\mathrm{pressure}}(y) = \left[\frac{c_{\mathrm{MW,C}}(x) + c_{\mathrm{MW,A}}(x)}{2}\right] \frac{k_\mathrm{P}}{\mu_\mathrm{W}(x)} \left(\frac{\partial p_{\#,\mathrm{vapor}}}{\partial y}\right) \tag{21}$$

where $p_{\#,\mathrm{vapor}}$ is the water vapor pressure in the anode and cathode channels, respectively. k_p the permeability of water in the membrane, $\mu_\mathrm{W}(x)$ the water viscosity and $c_{\mathrm{MW,C}}(x)$ and $c_{\mathrm{MW,A}}(x)$ are the concentrations of water in cathode and anode, respectively, with the expression given below [6]:

$$c_{\mathrm{MW},\#}(x) = \begin{cases} \dfrac{\rho_{\mathrm{m,dry}}}{M_{\mathrm{m,dry}}}[0.043 + 17.8a_\#(x) - 39.8a_\#^2(x) + 36.0a_\#^3(x)] & \text{for } 0 < a_\#(x) \le 1 \\ \dfrac{\rho_{\mathrm{m,dry}}}{M_{\mathrm{m,dry}}}[14 + 1.4(a_\#(x) - 1)] & \text{for } a_\#(x) > 1 \end{cases} \tag{22}$$

where $\rho_{\mathrm{m,dry}}$ and $M_{\mathrm{m,dry}}$ are the density and the equivalent weight of a dry proton exchange membrane. Therefore, the change of water flux along the channel at the cathode can be expressed by

$$\frac{\mathrm{d}N_{\mathrm{C,water}}(x)}{\mathrm{d}x} = [n_{\mathrm{H_2O}} I(x) + N_{\mathrm{drag}}(y) - N_{\mathrm{concentration}}(y) - N_{\mathrm{pressure}}(y)]h\alpha_{\mathrm{area}} \tag{23}$$

The variable trend of water flux in anode can be expressed by

$$\frac{\mathrm{d}N_{\mathrm{A,water}}(x)}{\mathrm{d}x} = [-N_{\mathrm{drag}}(y) + N_{\mathrm{concentration}}(y) + N_{\mathrm{pressure}}(y)]h\alpha_{\mathrm{area}} \tag{24}$$

The mole number of water condensation or evaporation can be calculated as [6]:

$$\frac{\mathrm{d}N_{\#,\mathrm{liquid}}(x)}{\mathrm{d}x} = \left(\frac{k_\mathrm{c} h d}{R_\mathrm{u} T_\#(x)}\right)\left[\frac{N_{\#,\mathrm{vapor}}(x)}{\sum_i N_{\#,i}(x)} p_\#(x) - p_{\#,\mathrm{sat}}(x)\right] \quad (i, \text{the gaseous species in stream \#}) \tag{25}$$

In order to present the state of vapor water and liquid water, relative humidity (RH) and relative water content (ϕ) are defined as follows:

$$\mathrm{RH}_\#(x) = \frac{\text{partial pressure of vapor water}}{\text{saturation pressure}} \quad \text{or} \quad \mathrm{RH}_\#(x) = \frac{N_{\#,\mathrm{vapor}}(x)}{\sum_i N_{\#,i}(x)} \frac{p_\#(x)}{p_{\#,\mathrm{sat}}(x)} \tag{26}$$

and

$$\phi_\#(x) = \frac{\text{mole number of water (vapor + liquid)}}{\text{mole number of water in saturation}} \quad \text{or} \quad \phi_\#(x) = \frac{N_{\#,\mathrm{water}}(x)}{\sum_i N_{\#,i}(x)} \frac{p_\#(x)}{p_{\#,\mathrm{sat}}(x)} \quad (i, \text{the gaseous species in stream \#}) \tag{27}$$

2.3. Energy balance

As shown in Fig. 3, the energy in a unit fuel cell consists of the energy released from chemical reactions, which is the source of energy in fuel cell; the electrical energy for generating power; the heat for increasing the solid phase temperature; the sensible heat for increasing the temperature of flow; the latent heat for water phase changes; the waste heat taken away by coolant; and the heat loss to the environment at the inlet and exit of channel.

The total energy balance is

$$q_{\mathrm{rxn}}(x) = q_{\mathrm{elec}}(x) + q_{\mathrm{heat}}(x) = q_{\mathrm{elec}}(x) + q(x)_{\mathrm{stack}} + \sum q_{\#,\mathrm{sen}}(x) + \sum q_{\#,\mathrm{latent}}(x) + q_{\mathrm{cool}}(x) \tag{28}$$

The energy released from electrochemical reaction is difficult to calculate. In general, enthalpy or entropy is employed to evaluate the energy and electrical work in an electrochemical system. For a reversible cell:

$$q_{\mathrm{heat}}(x) = T_0 \Delta S(x) \tag{29}$$

In this study, the entropy is used to calculate the released energy. For the reacting and non-reacting system, the entropy balance for undergoing any process can be expressed as

$$(S_{\mathrm{in}} - S_{\mathrm{out}}) + S_{\mathrm{gen}} = \Delta S_{\mathrm{system}} \tag{30}$$

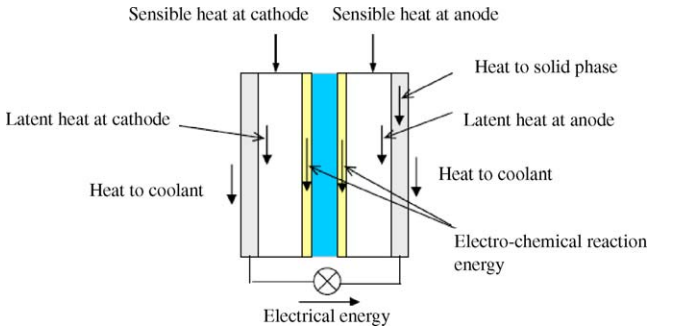

Fig. 3. Energy balance of a unit fuel cell.

This means that the change of entropy in a system can be determined by the net entropy transfer and the entropy generated in the system. The difference of the entropy change between a system with chemical reaction and a non-reacting system is that: the entropy relations for the reactants and the products involve the entropies of the components, not entropy changes, which is the case for non-reacting system [17]. Thus, a common base for the entropy of all substances is established by the third law of thermodynamics. Based on the third law of thermodynamics, the entropy has a common universal scale for each chemical compound. The common scale, called the absolute entropy, is based on the fact that the entropy for any pure element is zero at the temperature of absolute zero. For the electrochemical reaction in a PEM system, it is difficult to calculate the reaction heat for the total reaction. However, if one could tell the heat generation in which electrode heat is generated and in which it is absorbed, the corresponding total reaction heat can be calculated easily. For the electrode reaction at the anode, the entropy change can be calculated by

$$\Delta S_{\mathrm{A}}^{\circ} = 4S_{\mathrm{H^+}}^{\circ} + 4S_{\mathrm{e^-}}^{\circ} - 2S_{\mathrm{H_2}}^{\circ} \tag{31}$$

where S° is the absolute values of species at the standard state: $T_0 = 298.15$ K, $P_0 = 1$ bar. The numerical values for the species are taken from Refs. [18,19]. The entropy change at anode is: $S_{\mathrm{A}} = 0.208\ \mathrm{J\ (mol\ K)^{-1}}$ [18]. In the same way, the entropy change for the cathode reaction, can be calculated by

$$\Delta S_{\mathrm{C}}^{\circ} = 2S_{\mathrm{H_2O}}^{\circ} - S_{\mathrm{O_2}}^{\circ} - 4S_{\mathrm{e^-}}^{\circ} - 4S_{\mathrm{H^+}}^{\circ} \tag{32}$$

The entropy change at the cathode is: $S_{\mathrm{C}} = -326.36\ \mathrm{J\ (mol\ K)^{-1}}$ [18]. The absolute entropy of species i at temperature T and pressure P can be calculated from

$$S_i(T, P, x) = S_i^{\circ} + \int_{T_0}^{T} \frac{C_{p,i}(x)}{T}\,\mathrm{d}T + \int_{P_0}^{P} \left[-\frac{\partial v_i(x)}{\partial T(x)}\right] \mathrm{d}p \tag{33}$$

where $v_i(x)$ is the specific volume of flow at the location of x. Considering the total reaction in a cell, the reaction heat flux ($\mathrm{J\ s^{-1}}$) can be calculated for the reversible process as

$$q_{\mathrm{heat}}(x) = \left[\frac{\Delta S_{\mathrm{A}}(x)}{2F} + \frac{\Delta S_{\mathrm{C}}(x)}{4F}\right] T_{\mathrm{s}} I(x) h\alpha_{\mathrm{area}}\,\mathrm{d}x \tag{34}$$

For the real irreversible process, due to the ohmic loss and reaction resistance, some of the electrical energy is turn into the released heat. The total reaction heat flux can be expressed as

$$q_{\mathrm{heat}}(x) = \left[\frac{\Delta S_{\mathrm{A}}(x)}{2F} + \frac{\Delta S_{\mathrm{C}}(x)}{4F}\right] T_{\mathrm{s}} I(x) h\alpha_{\mathrm{area}}\,\mathrm{d}x - \eta(x) I(x) h\alpha_{\mathrm{area}}\,\mathrm{d}x \tag{35}$$

If the numerical value of $q_{\mathrm{heat}}(x)$ is negative, it means that the chemical reaction emits heat to the surrounding.

The electrical energy ($\mathrm{J\ s^{-1}}$) is

$$q_{\mathrm{elec}}(x) = V_{\mathrm{cell}}(x) I(x) h\alpha_{\mathrm{area}}\,\mathrm{d}x \tag{36}$$

The sensible heat of mixture flow at cathode channel ($\mathrm{J\ s^{-1}}$) is

$$\mathrm{d}q_{\#,\mathrm{sen}}(x) = \sum_i [N_{\#,i}(x) C_{p,i}(x)]\,\mathrm{d}T_{\#}(x) \quad (i, \text{the gaseous species in stream \#}) \tag{37}$$

The latent heat for water vapor condensation or liquid water evaporation at cathode or anode channels ($\mathrm{J\ s^{-1}}$):

$$\mathrm{d}q_{\#,\mathrm{latent}}(x) = [H_{\#,\mathrm{vapor}}(x) - H_{\#,\mathrm{liquid}}(x)]\,\mathrm{d}N_{\#,\mathrm{liquid}}(x) \tag{38}$$

In this model, the heat taken by the coolant is considered and expressed by

$$q_{\mathrm{cool}}(x) = U_{\mathrm{cool}} A_{\mathrm{cool}} [T_{\mathrm{S}}(x) - T_{\mathrm{cool}}] \tag{39}$$

where U_{cool} is the heat transfer coefficient between stack and coolant, A_{cool} is the area of heat transfer.

When the streams flow along the channels, they will gain or lose heat due to the heat transfer between the fluid and stack. Therefore, the temperature of flow depends on the stack temperature and the latent heat as well, which can be calculated as follows:

$$\sum_i [N_{\#,i}(x) C_{p,i}(x)] \frac{\mathrm{d}T_{\#}(x)}{\mathrm{d}x} = [H_{\mathrm{W,vapor}}(x) - H_{\mathrm{W,liquid}}(x)] \frac{\mathrm{d}N_{\#,\mathrm{liquid}}(x)}{\mathrm{d}x} + U_{\#} h [T_{\mathrm{S}}(x) - T_{\#}(x)] \tag{40}$$

$U_{\#}$ represents the heat transfer coefficient between the flow stream # and stack. The term on left side of the equation represents the heat flux obtained by gaseous flows. The first term on the right side of the equation accounts for the enthalpy change due to condensation or evaporation of water in the channels, which can be calculated using Eq. (41). The second term on the right side of the equation is for the convection heat flux between the stream and the stack:

$$\begin{aligned} H_{\#,\mathrm{vapor}}(x) - H_{\#,\mathrm{liquid}}(x) &= 45070 - 41.9[T_{\#}(x) - 273] + 3.44 \times 10^{-3}[T_{\#}(x) - 273]^2 \\ &\quad + 2.54 \times 10^{-6}[T_{\#}(x) - 273]^3 \\ &\quad - 8.98 \times 10^{-10}[T_{\#}(x) - 273]^4 \end{aligned} \tag{41}$$

The stack temperature varies with position/location along the channels. It is determined by the local current density, local latent heat, and local cooling heat. It is calculated by the following energy balance equation:

$$\begin{aligned} A_S k\frac{d^2T_S(x)}{dx^2} &- [N_{C,liquid}(x)+N_{A,liquid}(x)]C_{P,water}\frac{dT_S(x)}{dx} \\ &= -A_C U_{\#}[T_A(x)+T_C(x)-2T_S(x)] \\ &\quad - A_{cool}U_{cool}[T_{cool}(x)-T_S(x)] \\ &\quad - [H_{A,vapor}(x)-H_{A,liquid}(x)]\frac{dN_{A,liquid}(x)}{dx} \\ &\quad - [H_{C,vapor}(x)-H_{C,liquid}(x)]\frac{dN_{C,liquid}(x)}{dx} \\ &\quad + \left[\left(\frac{\Delta S_A(x)}{2F}+\frac{\Delta S_C(x)}{4F}\right)T_S(x)-\eta(x)\right]I(x)h\alpha_{area} \end{aligned} \tag{42}$$

where k is the thermal conductivity of the stack, A_S the cross-section area of the stack along the flow direction, A_C the heat transfer area between stack and flows, and A_{cool} is the heat transfer area between stack and coolant. The term on the left side of equation represents energy flow by the conduction in the stack of the cell along the gas flow path (x-direction). The temperature distribution normal to gas flow (y-direction) is assumed to be uniform. The first term on the right side of equation is for convective heat transfer between the streams in the channels and the cell stack. The second term on the right side of equation accounts for convective heat transfer between the cell stack and coolant. The temperature of coolant is assumed to be constant along the channels. The third and fourth terms represent the energy taken or released from the phase changes of water in the anode or cathode flow (latent heat), which can be calculated in Eq. (40). The last term represents heat generation by the reversible chemical reaction process.

2.4. Pressure drop

The pressure drop of the gas mixture in the fuel cell flow channel was rarely considered in currently available fuel cell research publications. But, in industrial design and practice, it is a significant parameter simply because it directly affects system efficiency.

The saturation pressure (Pa) can be expressed in terms of the local temperature [19]:

$$p_{sat}(x) = 1.013\times10^5\times10^{-2.1794+0.02953(T_{\#}(x)-273)-9.1837\times10^{-5}(T_{\#}(x)-173)^2+1.4454\times10^{-7}(T_{\#}(x)-273)^3} \tag{43}$$

Based on the assumption that the mixture is regarded as an ideal gas, local volumetric flow ($m^3\,s^{-1}$) in the cathode and anode can be calculated using the ideal-gas law:

$$Q_{\#}(x) = \sum_i N_{\#,i}(x)R_u\frac{T_{\#}(x)}{p_{\#}(x)}$$
(i, the gaseous species in stream #) (44)

The local velocity ($m\,s^{-1}$) in the cathode and anode can be calculated as follows:

$$V_{\#}(x) = \frac{Q_{\#}(x)}{A_{\#,cross}} \tag{45}$$

where $A_{\#,cross}$ is the cross-section area of channel.

Since the mole fraction of gases in the channel varies, local density ($kg\,m^{-3}$) also varies with the different components in the flow. It can be calculated from

$$\rho_{\#}(x) = \sum_i\left[\frac{N_{\#,i}(x)}{\sum_i N_{\#,i}(x)}\frac{M_{\#,i}}{1000}\right]\frac{p_{\#}(x)}{T_{\#}(x)R_u}$$
(i, the gaseous species in stream #) (46)

Local dynamic viscosity can be calculated by interpolation. $\mu_{i,100}$ is the gas dynamic viscosity at 100 °C and $\mu_{i,0}$ is the gas dynamic viscosity at 0 °C. The temperature range of flow in the calculated cases is 0–100 °C, so, the local dynamic viscosity is

$$\mu_{\#}(x) = \sum_i\left\{\frac{N_{\#,i}(x)}{\sum_i N_{\#,i}(x)}\left[\frac{T_{\#}(x)-273}{100-0}(\mu_{i,100}-\mu_{i,0})+\mu_{i,0}\right]\right\}$$
(i, the gaseous species in stream #) (47)

For laminar flow, pressure drop in each control volume can be expressed as (Pa):

$$\frac{dp_{\#}(x)}{dx} = \rho_{\#}(x)f_{\#}(x)\frac{V_{\#}^2(x)}{2D} \tag{48}$$

where $f_{\#}(x)$ is the friction factor and D the hydraulic diameter of the channel. In this model, the channels are straight, so that only friction loss is considered. The local pressure (Pa) is calculated from the pressure at inlet by subtracting the pressure drop from the inlet to the current control volume:

$$p_{\#}(x) = p_{\#,in} - \int_0^x\left[\frac{dp_{\#}(x)}{dx}\right]dx \tag{49}$$

The total required pumping power (W) is used by the designer to choose a pump to maintain the flow. It is given by

$$P_{\#,pump} = N_{ch}\int_0^L\frac{dp_{\#}(x)}{dx}Q_{\#}(x)\,dx \tag{50}$$

2.5. Cell output voltage

Cell output voltage is a significant parameter that is used to evaluate the performance of a PEM fuel cell. The goal in this section is to model the potential losses in the gas diffusion layers and membrane, so that the output potential can be accurately predicted. The output voltage of the fuel cell is modeled as

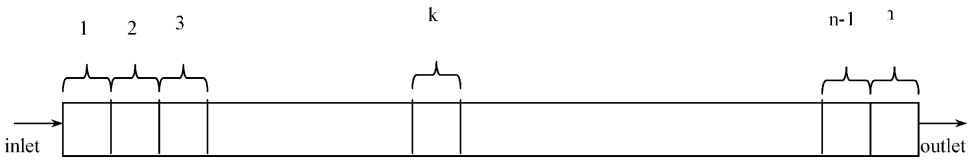

Fig. 4. Control volume layout for numerical solution along the channel.

the reversible cell voltage minus activation losses, concentration over-potential and ohmic resistance of the electrodes, catalyst layer and membrane. The cell potential is expressed as [6]:

$$V_{\text{cell}} = V_{\text{oc}} - \eta(x) - \frac{I(x)t_{\text{m}}}{\sigma_{\text{m}}(x)} \tag{51}$$

where V_{oc} is the open-circuit potential of fuel cell and $\eta(x)$ refers to the cell over-potential which combines activation losses and concentration losses together and is calculated as follows [6]:

$$\eta(x) = \frac{R_{\text{u}}T_{\text{s}}(x)}{0.5F}\ln\left(\frac{I(x)}{I^0 p_{\text{C,O}_2}(x)}\right) \tag{52}$$

where I^0 is the exchange current density at one atmosphere of oxygen, $p_{\text{C,O}_2}(x)$ the partial pressure of oxygen at cathode, $\frac{I(x)t_{\text{m}}}{\sigma_{\text{m}}(x)}$ the ohmic loss which depends on the membrane water activity, stack temperature and membrane thickness and $\sigma_{\text{m}}(x)$ is the membrane conductivity calculated by the following equation [19]:

$$\sigma_{\text{m}}(x) = \left(0.00514\frac{M_{\text{m,dry}}}{\rho_{\text{m,dry}}}c_{\text{MW}}(x) - 0.00326\right) \times\exp\left(1268\left[\frac{1}{303} - \frac{1}{T_{\text{s}}(x)}\right]\right) \tag{53}$$

where

$$c_{\text{MW}}(x) = \begin{cases} \dfrac{\rho_{\text{m,dry}}}{M_{\text{m,dry}}}[0.043 + 17.8a(x) - 39.85a^2(x) + 36.0a^3(x)] & \text{for } 0 < a(x) \le 1 \\ \dfrac{\rho_{\text{m,dry}}}{M_{\text{m,dry}}}[14 + 1.4(a(x) - 1)] & \text{for } a(x) > 1 \end{cases} \tag{54}$$

The current density is distributed unevenly along the channel. However, when a fuel cell is evaluated, the output current is of major concern. Therefore, the average current density is calculated using:

$$I_{\text{avg}} = \frac{1}{L}\int_0^L I(x)\,\mathrm{d}x \tag{55}$$

3. Solution procedure

Based on previous analysis, the model can be summarized into a set of non-linear differential equations. In this study, iterative methods are chosen to solve the differential equations. The solution procedure includes three loops. The outer loop adopts a Gauss–Jacobi method to solve the equations, such as mass of hydrogen, mass of oxygen, pressure drop, stream temperatures, mass of water vapor and liquid water, and so on. In the inner loop, a Tri-Diagonal Matrix Algorithm is used to calculate the energy balance to get the stack temperature. For the non-linear algorithm equation, such as cell potential–current density

Table 1
Geometry parameters of a single fuel cell.

Parameters	Values
Channel length (L)	85 cm
Channel width at cathode and anode (h)	0.15 cm
Channel height at cathode and anode (d)	0.08 cm
Channel number of cathode and anode (N_{ch})	6
The effective area	100 cm^2
Condensation rate constant (k_{c})	1.0 s^{-1}
Membrane dry density ($\rho_{\text{m,dry}}$)	2.0 g cm^{-3}
Membrane dry equivalent weight ($M_{\text{m,dry}}$)	1100 g mol^{-1}
Membrane thickness (t_{m})	0.01275 cm
Fuel cell open-circuit voltage (V_{oc})	1.1 V
Oxygen exchange current density (I^0)	0.01 A cm^{-2}
Diffusion coefficient of water in membrane (D^0)	5.5×10^{-7} $\text{cm}^2\ \text{s}^{-1}$

Eq. (51), the Newton–Raphson method is applied to calculate the local current density. Before the iterative methods can be applied, the differential equations are required to be discretized into algebraic equations. In this simulation, the finite difference method is adopted. The channel is subdivided into n control volumes of equal length $L = L/n$ in x-direction (shown in Fig. 4). The exit values at the kth control volume are the inlet values at the $(k+1)$th control volume, and all variables are stored at the centroid of each cell. A set of differential equations is replaced by algebraic equations based on this method.

In this simulation, the hydrogen and air flow in the channels are in the coflow mode. Table 1 lists the basic geometric parameters and electrode and membrane properties of the unit fuel cell.

4. Model validation and results analysis

A Nexa$^{\text{TM}}$ system [20] is used in this experiment. The Nexa$^{\text{TM}}$ system consumes hydrogen and air to provide dc power up to 1200 W with a nominal output voltage of 26 VDC. It contains a BALLARD® fuel cell stack, as well as all the auxiliary equipment necessary for fuel cell operation.

Fig. 5 compares the simulation results for constant stack temperature and for variable stack temperature with the experimental data. When the current density is less than 0.25 A cm^{-2}, the output voltage in the modes is greater than the experimental results. After the current density exceeds 0.3 A cm^{-2}, the output voltage in the model is less than the experiment results.

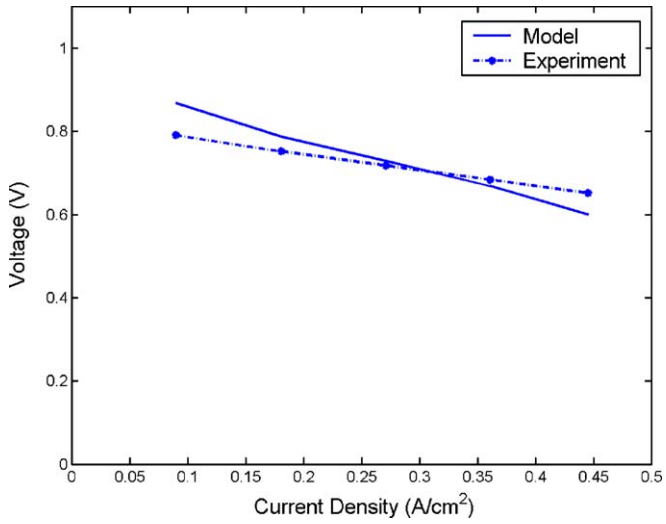

Fig. 5. Comparison of the model predictions with the empirical data.

Obviously, the inner resistances in the models are greater than that in practice. Meanwhile, the resistance in the constant stack temperature model is greater than that in the variable stack temperature model. It is difficult to explain clearly the exact reasons for the errors between the model results and experiment results. However, some factors may contribute to the error of the resistance calculation, which lead to the above simulation result.

In the model, $\frac{I(x)t_m}{\sigma_m(x)}$ represents the ohmic loss inside the fuel cell, which depends on local current density, membrane thickness, and the membrane conductivity. The experimental equation for membrane conductivity comes from experimental results of Ref. [21], which is based on a fully hydrated membrane of Nafion 117. In the real situation, at many local points of membrane, the hydration is not perfect, which means the water activity in membrane varies. In addition, at the time of this report, data on the material and membrane thickness for the Nexa™ power module was not available. According to previous research [22], the material and thickness of the membrane affect the membrane conductivity greatly. Without the detailed information regarding the membrane, it is challenging to obtain agreeable curves between model results and experimental results.

4.1. Base case analysis

The simulation is based on an operating condition at near room temperature and low pressure, which is called the "Base case". The detailed operating conditions of the base case are listed in Table 2.

Fig. 6 shows the local current density in the base case along the channel. The current density is highest at the channel inlet. It then drops quickly to the lowest point. After that, current density increases slowly along the channel until it reaches the channel exit, where the current density increases sharply. This observation could be attributed to membrane water activity changes along the channel.

Fig. 7 shows the water activity in the cathode flow, anode flow and membrane, respectively. Near the channel inlet, the water vapor in the flow is sufficient and the membrane is well hydrated,

Table 2
Operating condition in base case

Parameters	Values
Inlet temperature of air	313 K
Inlet temperature of hydrogen	313 K
Inlet relative humidity of air	1.0
Inlet relative humidity of hydrogen	1.0
Outlet pressure of cathode	109535 Pa
Outlet pressure of anode	109535 Pa
Current density	0.5 A cm^{-2}
Excess coefficient of flow at cathode	2.02
Excess coefficient of flow at anode	1.169

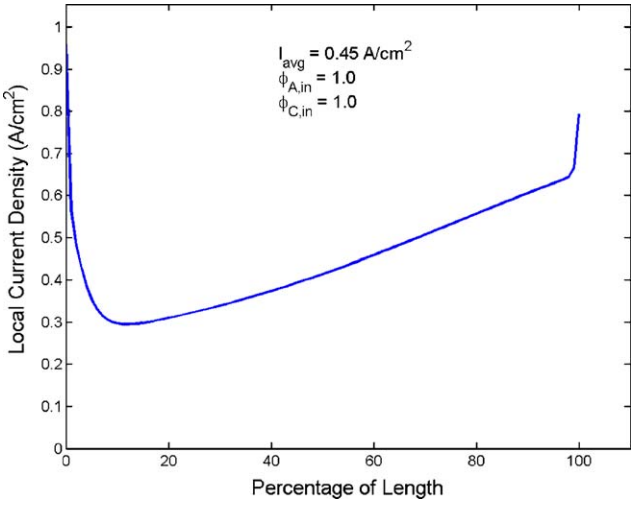

Fig. 6. The distribution of current density along channel in the base case.

which increases the local conductive and electro-osmotic drag coefficient of the membrane. As a result, more hydrogen ions can pass through the membrane and generate higher current density. Further down the channel, the water activity at the anode flow drops quickly and the membrane becomes drier and more resistive which decreases the current density. However, since there is some water produced by the electrochemical reac-

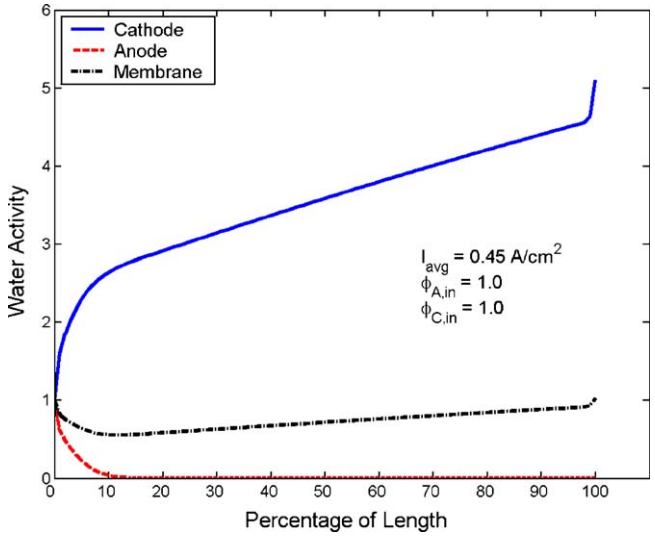

Fig. 7. The distribution of water activity along channel in the base case.

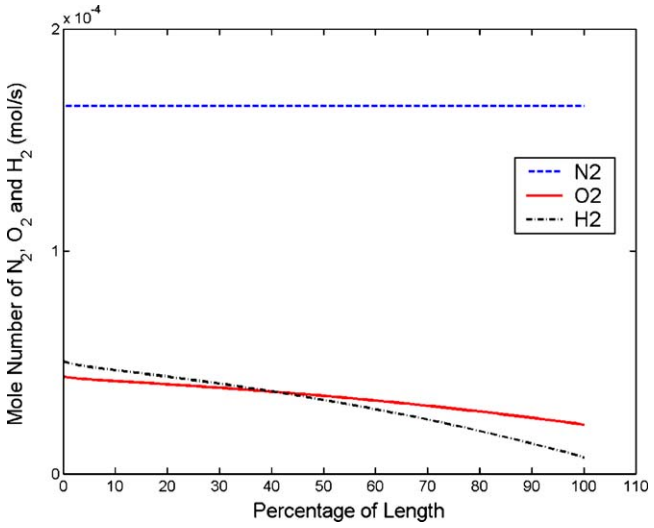

Fig. 8. The distribution of hydrogen, oxygen and nitrogen along channel in the base case.

tion continually at the cathode, the water activity of the stream increases gradually along the channel. Correspondingly, the current density increases. In summary, the water vapor fraction in the flow has a direct impact on fuel cell performance. Fig. 9 also displays that the water activity in the membrane depends on the water activity in both the cathode and anode streams.

Fig. 8 shows how the mole number of oxygen and hydrogen decrease along the channel. Since the excess coefficient of air is higher than that of hydrogen, the molar fraction of oxygen is larger than that of hydrogen at the channel exit. The reason for choosing a large excess coefficient of air is that the excess air is needed to take away the extra water in the cathode channel. The mole number of nitrogen does not change because it is not involved in the electrochemical reaction.

Fig. 9 shows the relationship of water activity, water content and water relative humidity in channels which have been defined in the model description section above. In the cathode channel, the relative humidity of stream is equal to 1.0. Because the water is produced continually, the water activity and water content keep increasing. When the water vapor partial pressure is greater than the saturation pressure, water vapor will condense to liquid water. If the water vapor condensation rate is too low, the water vapor partial pressure can be greater than the saturation pressure in a short period of time. Therefore, the water activity can be greater than 1.0. According to their definitions, the difference between the water activity curve and water content curve at some point indicates that there is liquid water in this part of the channel. In the anode channel, since the flow is usually unsaturated and there is no liquid water along the channel, the three curves are overlapped. Fig. 10 shows the relationship between water content and water activity when the anode inlet water content is 1.25 and the liquid water is injected into the anode channels. In this special case, although relative humidity along the channels is no more than 1.0, it still can be seen that the water content curve and water activity curve are not overlapped. The area between water content and water activity means that liquid water exists in the channels. This phenomenon is due to the lower liquid water evaporation rate. Meanwhile, it is found that the water content curve and water activity curve overlap after 60% of the channel length. This behavior is attributed to the fact that all of the liquid water evaporates into water vapor at this location. Therefore, beyond this point, there is no liquid water in the channel.

Fig. 11 shows the temperature distribution of the cathode stream, the anode stream and the stack along the channel. Fig. 12 gives the detailed temperature curves in the vicinity of the inlet. At this part of the channel, heat can be transferred from the stack to the environment by convection, which leads to the stack temperature being lower than the stream temperature. Further down the channel, there are several heat transfer processes taking place: (a) a chemical reaction occurs and reaction heat is released to the solid stack; (b) water vapor condenses and latent heat is released; (c) convection heat transfer occurs as well due to the temperature difference between the stream and stack.

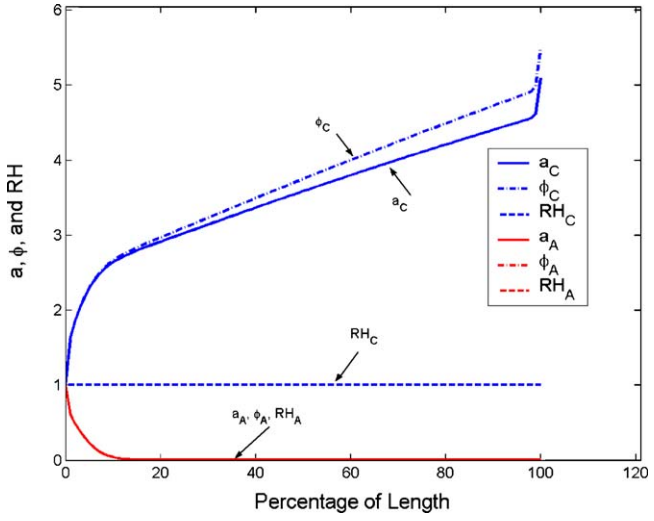

Fig. 9. The water activity, water content and relative humidity along channel in the base case.

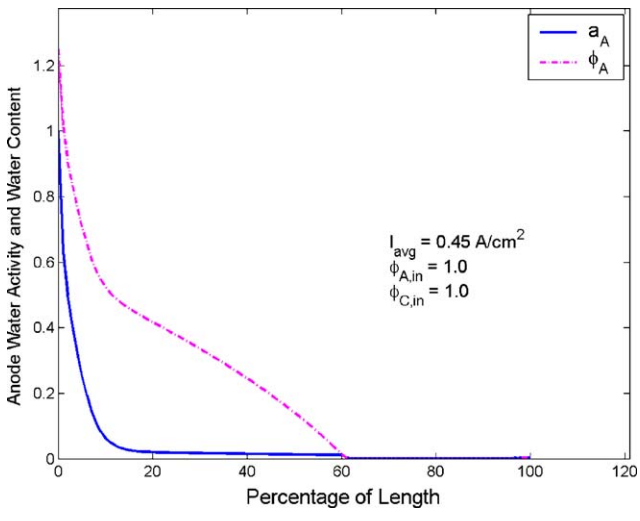

Fig. 10. The water activity, water content along channel for the liquid water injection case.

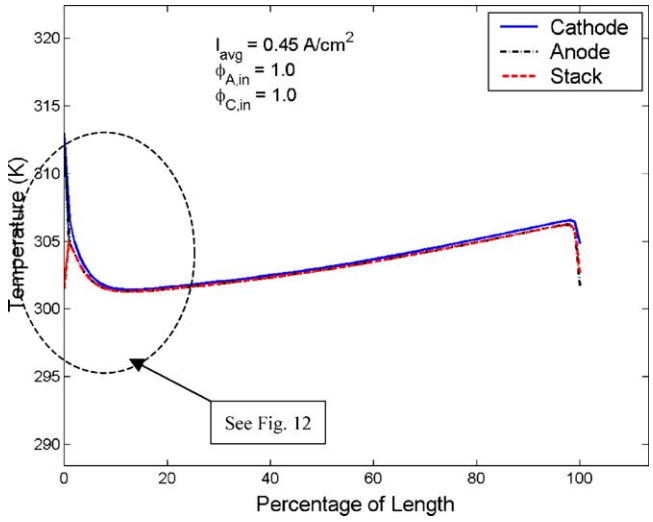

Fig. 11. The distribution of temperature along channel in the base case.

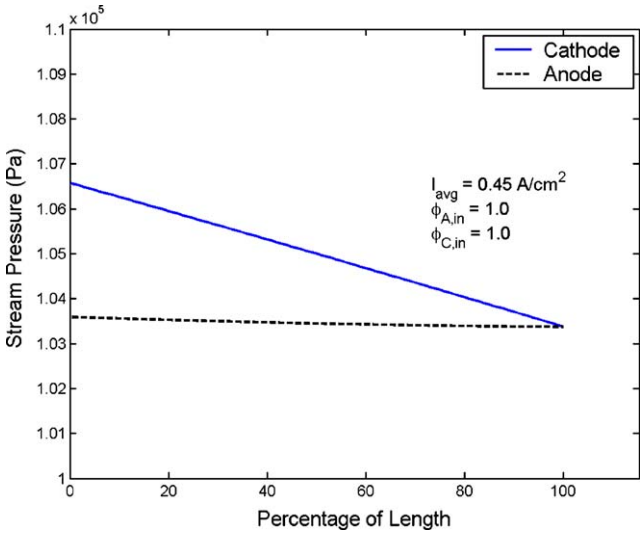

Fig. 13. Distribution of pressure along channels in the base case.

According to the curve, the anode temperature drops quickly near the channel inlet. When it reaches the stack temperature, it increases with stack temperature. The cathode temperature drops slowly, at 15% of the channel length, it reaches the same temperature as the stack. It can be observed that the large flowrate leads to the flow temperature changing slowly at the cathode.

Fig. 13 shows the distribution of pressure along the channel. Obviously, the pressure drop at the cathode channel is larger than that at the anode channel. This is because the flowrate at cathode increases, which increases the flow velocity as well. On the other hand, the flowrate and velocity of the stream at the anode decreases, consequently, the pressure drop decreases.

4.2. *Influence of the inlet temperatures of reactant gases*

In this section, the effects of inlet temperatures of flow on the PEM fuel cell performance will be evaluated. The inlet temperatures of flows at both anode and cathode are set to 303, 313, 323, 333, and 343 K, respectively.

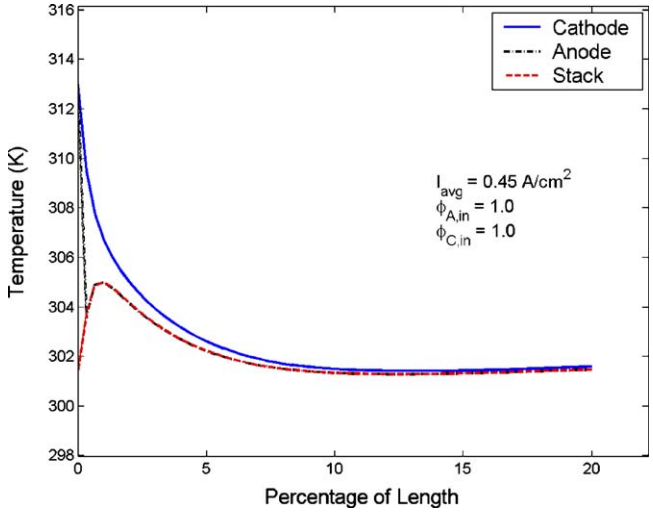

Fig. 12. The distribution of temperature at the inlet of channel in the base case.

The distribution of current density with different inlet temperatures is shown in Fig. 14. The distributions of current density are totally different for each inlet flow temperature. When the inlet temperatures of flow are 303 and 313 K, the values of current densities are highest at the channel inlet. They then decrease quickly until they reach the lowest point at around the 8% of length down the channel. After that, the current density increases again. The distribution of current density is very interesting when the inlet temperature of flow is 323 K. The current density increases slightly around the entrance, and then begins to drop along the channel. At approximately 10% of channel length, the current density reaches the lowest value. After that, the current density starts to increase again. This upward tendency stops at the position of about 60% of the channel length. When the inlet temperatures of flow are 333 and 343 K, the current densities increase near the inlet, and then keep decreasing until the channel exit. This occurs primarily because the current density depends on the water activity in the mem-

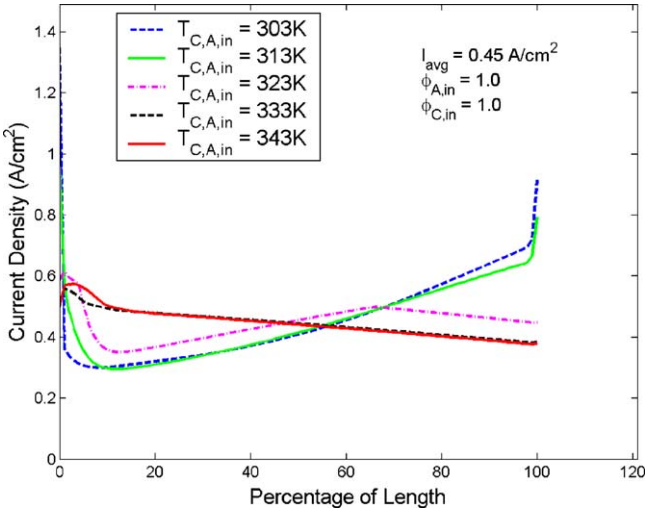

Fig. 14. A comparison of current profiles along the channels with the different inlet stream temperatures.

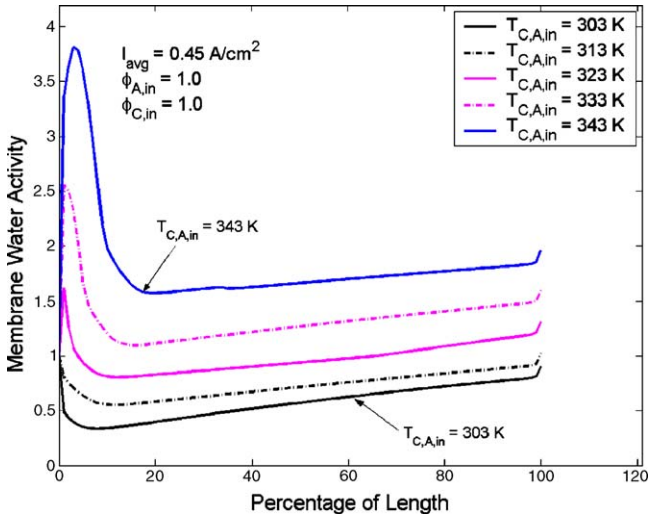

Fig. 15. A comparison of membrane water activity along the channels with the different inlet stream temperatures.

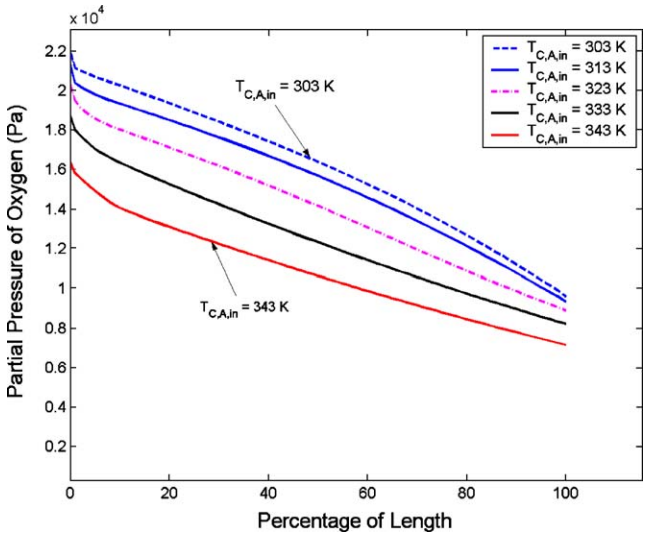

Fig. 16. A comparison of partial pressure of oxygen along the channels with the different inlet stream temperatures.

brane and the partial pressure of oxygen in the cathode stream. At a low inlet temperature, since the gas carries little water vapor, water activity is the primary factor that affects the current density.

Fig. 15 shows the distribution of water activity at the different inlet flow temperatures. It is found that the local water activities in the membrane are less than 1.0 when the inlet flow temperatures are 303 and 313 K. At a position around the 8% of the length down the channel, the water activity in the membrane reaches the lowest point. This means the membrane is very dry and the speed of electrochemical reaction is slow. Consequently, only a small number of electrons is produced, which leads to lower current density. With increasing membrane water activity along the channel, more hydrogen ions pass through the membrane and therefore, the current density increases. It is also noticeable that the membrane activity increases quickly near the channel exit. This can be explained due to the fact that the stack loses heat to the environment, which quickly lowers the stack temperature and flow temperatures. According to Eq. (43), the saturation pressure will drop and the water activities will increase. For the cases with higher inlet temperature, such as, 333 and 343 K, the gases carry more water vapor into the channel. Fig. 15 shows that the water activity in the membrane along the whole channel is greater than 1.0. According to Eq. (53), the membrane conductivity changes are small when water activities are large enough. Thus, the membrane is well hydrated and the speed of electrochemical reaction is fast. As a result, more oxygen is consumed and the partial pressure of oxygen decreases quickly (shown in Fig. 16). This effect contributes to the drop of the current density along the channel. When the inlet temperature is 323 K, the current density depends on both membrane water activity and partial pressure of oxygen. From the channel entrance to about 60% of channel length, the membrane water activity is less than 1.0. The current density changes with the increasing membrane water activity. When the membrane water activity is greater than 1.0, the membrane conductivity does not change much. However, the partial pressure of oxygen decreases quickly and consequently, the current density drops beyond 60% of the channel length.

Fig. 17 shows that increasing the inlet temperature of flow yields a higher cell potential. This behavior is attributed to the fact that the flow with high temperature introduces more water into the channel and membrane resistance decreases due to the hydration. It is noticed that the polarization curves at the inlet flow temperatures of 333 and 343 K are overlapped. This is because the membrane resistance remains basically constant when the membrane is well hydrated (water activity is greater than 1.0 along the whole channel).

Fig. 18 shows the stack temperature distributions. It can be seen that the tendency of stack temperature is similar to that of current density. The larger the current density is, the more the reaction heat is released and the higher the stack temperature. Fig. 19 shows that the inlet temperatures of flow have a great

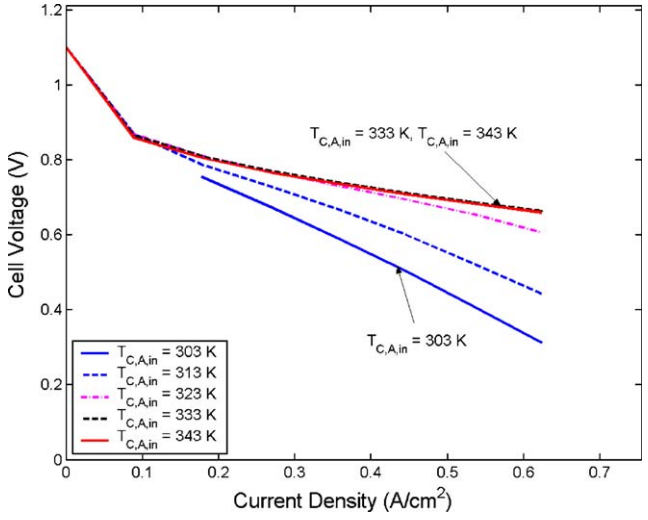

Fig. 17. The effect of inlet stream temperatures on the performance of a single PEM fuel cell.

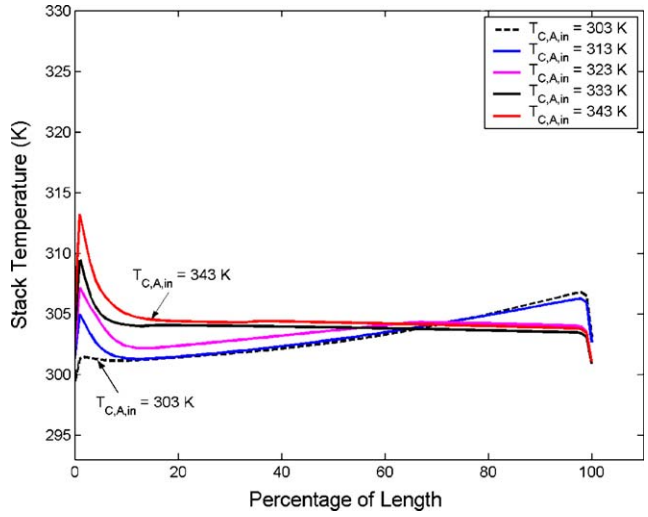

Fig. 18. The effect of inlet stream temperatures on stack temperature of a single PEM fuel cell.

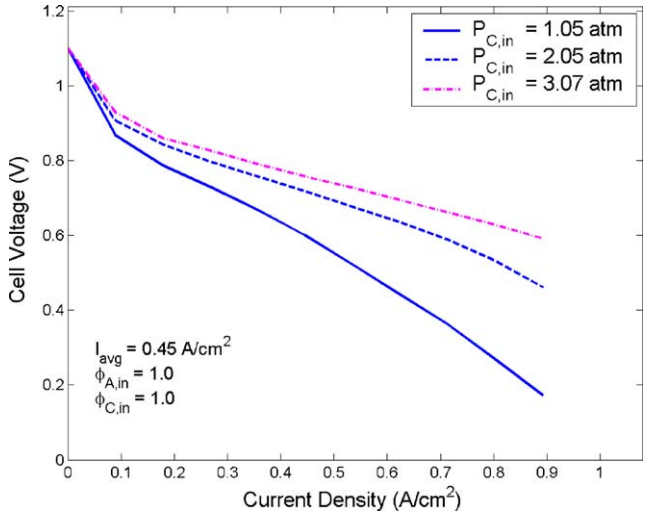

Fig. 20. The effect of pressure on the performance of a single PEM fuel cell.

effect on the pressure change along the cathode channels. When the inlet flow temperature is high, the speed of electrochemical reaction increases and more air is required. Thus, the flowrate in the cathode channels increase and the pressure drop increases as well.

4.3. Influence of pressure

Fig. 20 shows how the pressure affects the performance of a PEM fuel cell under various current densities. Over the entire range of the investigated current densities, a higher pressure leads to higher performance of the fuel cell. However, the potential difference between 1 and 2 atm is greater than that between 2 and 3 atm. Furthermore, this effect is more obvious when the current density is high. This is because the high-pressure streams can bring more water into the channel (shown in Fig. 21). As a result, the membrane is better hydrated and the speed of chemical reaction increases. Therefore, the fuel cell can generate more power under the high flow pressure. From the above analysis, a conclusion can be drawn that a high inlet gas pressure has a positive effect on system performance of fuel cell. However, whether to use the high pressure in a real fuel cell design depends on the trade off between system improvement and the cost of providing compressed gas.

4.4. Influence of coolant temperature

Generally, the fuel cell system has cooling equipment to remove waste heat and keep the fuel cell working under optimal conditions. To simulate this kind of situation, it is required to investigate how the coolant temperature affects the fuel cell performance. To keep it simple, the coolant temperature is assumed to be constant. In order to study the effect on heat removal, the polarization curves with different coolant temperature, which

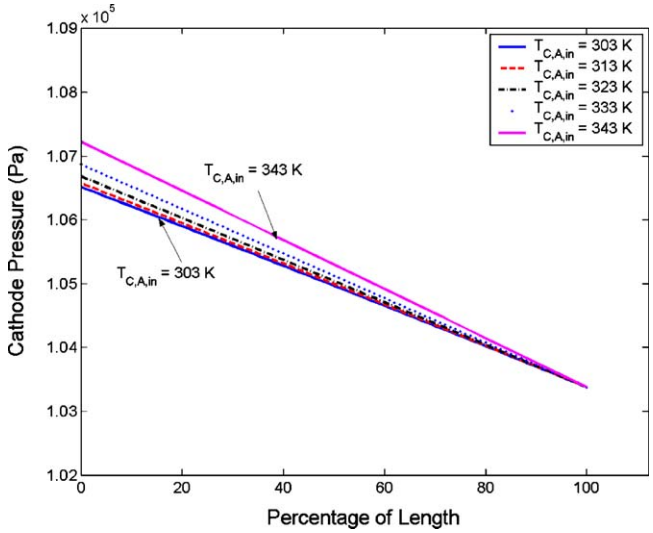

Fig. 19. The effect of inlet stream temperatures on cathode pressure of a single PEM fuel cell.

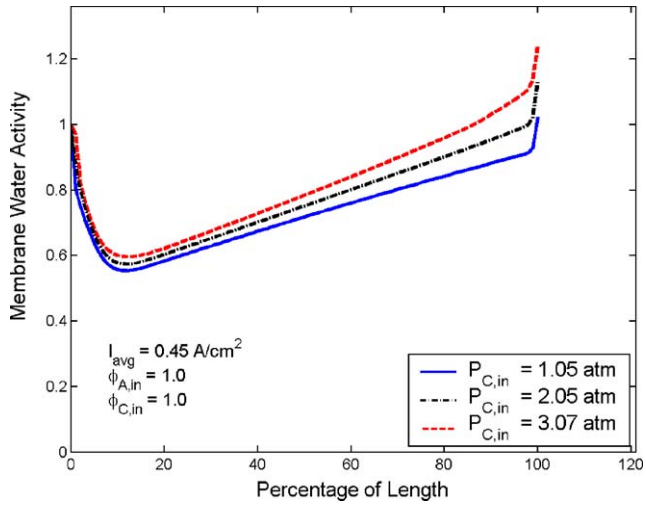

Fig. 21. The effect of pressure on membrane water activity of a single PEM fuel cell.

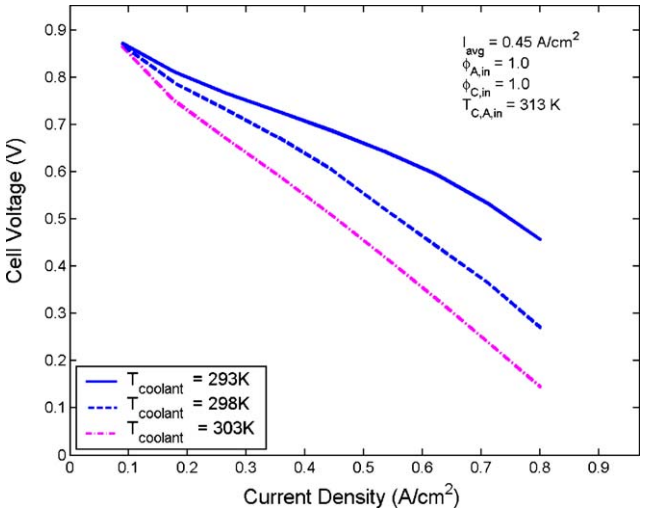

Fig. 22. The effect of coolant temperature on the performance of a single PEM fuel cell.

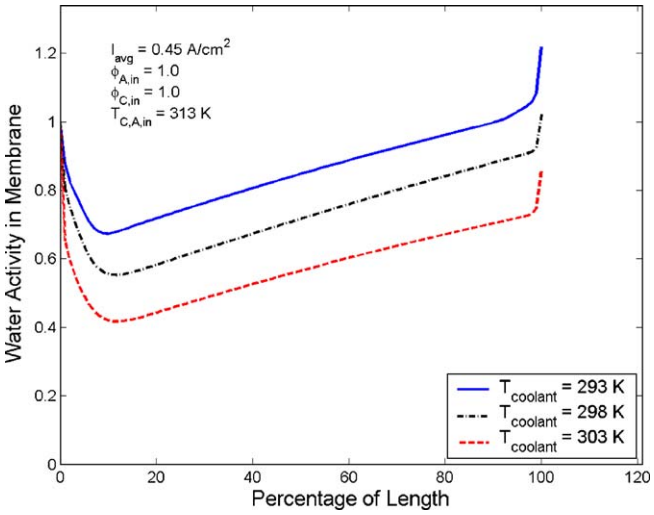

Fig. 24. The effect of coolant temperature on membrane water activity of a single PEM fuel cell.

are 293, 298, and 303 K, respectively, are plotted in Fig. 22. The operating conditions of the fuel cell are: the flow inlet temperature at 313 K and average current density at 0.45 A cm^{-2}. As can be observed, the lower the cooling air temperature is, the better fuel cell performance can be. The reason behind this phenomenon is quite simple. As the coolant temperature becomes lower, more heat can be taken away from the stack, which reduces the stack temperature. As the stack temperature goes down, so do the flow temperatures due to the intensified heat transfer between them (shown in Fig. 23). As the flow temperature becomes lower, the saturation pressure of water vapor drops which leads to an increase in the water activities. According to Fig. 24, the water activity in the membrane reaches the highest when the coolant temperature is at the lowest point. Therefore, the membrane is better hydrated and the speed of electrochemical increases. As a result, the performance of the fuel cell is improved as well.

4.5. *Influence of anode inlet humidification*

Water starvation in the anode channel is one of the problems that fuel cell designers have to face. As shown in the base case (Fig. 7), the anode and its interface with the membrane become less hydrated as the flow travels along the channels. This is because the water vapor at the anode is carried away by hydrogen ions and transported into the cathode. One way to solve this problem is to inject liquid water into the anode channel. As the flow at the anode becomes unsaturated, liquid water will evaporate to replenish the water loss. Therefore, the membrane is well hydrated. Fig. 25 illustrates variation of the amount of liquid water along the channel. It shows that the liquid water disappears at about 25% of the channel length when the inlet water content at the anode is 1.1. If the anode inlet water content increases to be 1.5, the liquid water will exist in the whole channel. This conclusion can be helpful in choosing the optimal anode inlet water content during fuel cell design.

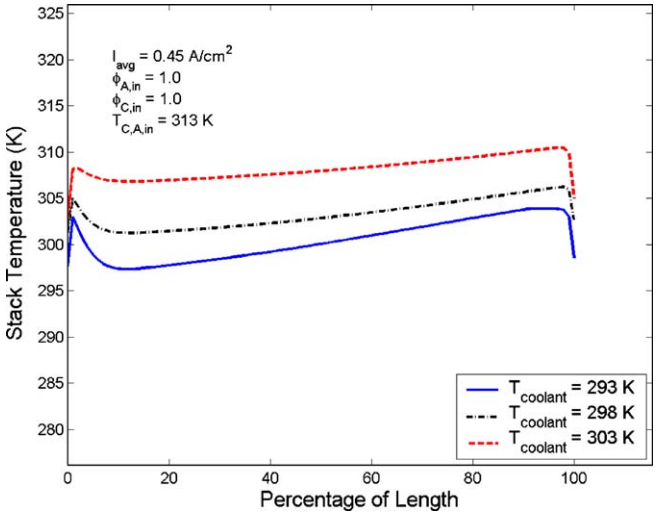

Fig. 23. The effect of coolant temperature on stack temperature of a single PEM fuel cell.

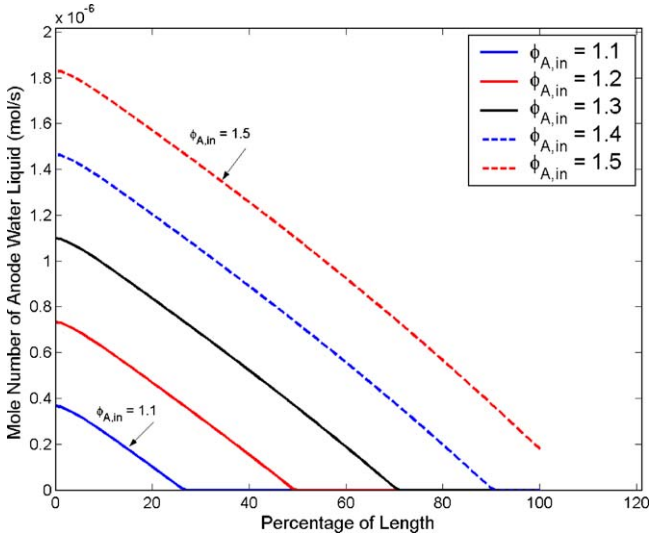

Fig. 25. A comparison of liquid water vary along the channels.

4.6. Constant stack temperature case analysis

In many previous studies, the stack temperature of the PEM fuel cell is assumed to be constant. However, this temperature is more likely to be variable in real operation. To investigate how the assumption of the constant stack temperature affects the accuracy of the simulation, a constant stack temperature case was simulated and the results compared with those discussed above. In this section, the Uniform Stack Temperature can be referred to as "UST" while the Non-Uniform Stack Temperature is labeled as "NST".

Figs. 26 and 13 show the temperature changes along the channel for UST case and NST case, respectively. In UST case, the stream temperature at the anode is the same as the stack temperature, since no reaction occurs and no heat is generated. Most of the reaction heat is taken away by the stream in the cathode channel. Obviously, this case is hardly true in real situations. The curves in Fig. 13 are more complex, since the reaction heat was taken into account. Here, the anode stream temperature is also close to the stack temperature but changes along the channel. As the speed of local reactions change, the local temperature of the cathode channel changes considerably as well. In other words, the temperature fields of the UST case in both the cathode and anode channels are quite different to those of NST case.

Fig. 27 shows the local current density of the base case along the channel for the UST case. As in the case of the corresponding curve in Fig. 6 for NST case, the current density is highest at the channel inlet. Then, it rapidly drops to its lowest point. After that, current density increases slowly along the channel. Unlike the NST case, there is no sudden increase of current density at the channel exit. This can be explained by water activity changes which have been presented in Fig. 28 for the UST case and Fig. 7 for the NST case. Contrary to the NST case, there is no large increase of water activity at the end of the channel when the stack temperature is constant. Therefore, the current density value does not jump at the channel exit since it is directly influenced by the water activity. In summary, the variable stack temperature can significantly affect the flow field and thermodynamic parameters inside the channel. Its influence on flow mode and energy conversion efficiency can hardly be ignored. Also, in the PEM model simulation, choosing a right boundary condition assumption is very important.

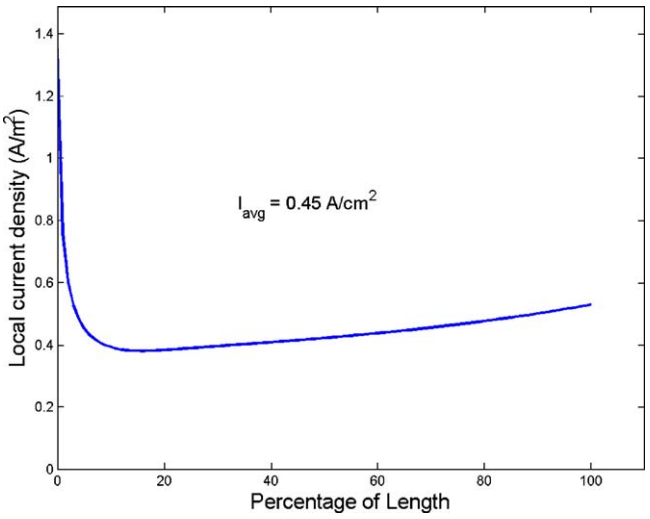

Fig. 27. Current density distribution along the channel in the base case of constant stack temperature.

The inlet temperatures of flow have an impact on the PEM fuel cell performance. Fig. 29 shows that a higher inlet temperature of flow yields a higher cell potential. As discussed before, this is mainly attributed to the fact that the flow with high temperature introduces more water to the channel and decreases the membrane resistance due to the hydration. The distribution of current density with different inlet temperatures is shown in Fig. 30. It is known that the current density depends on both the water activity in the membrane and the partial pressure of oxygen in the cathode stream. Figs. 31 and 32 show water activity in the membrane and the partial pressure of oxygen along the channel. At low inlet temperature, since the gas carries little water, the membrane is dry and the speed of electrochemical reaction is slow. As a result,

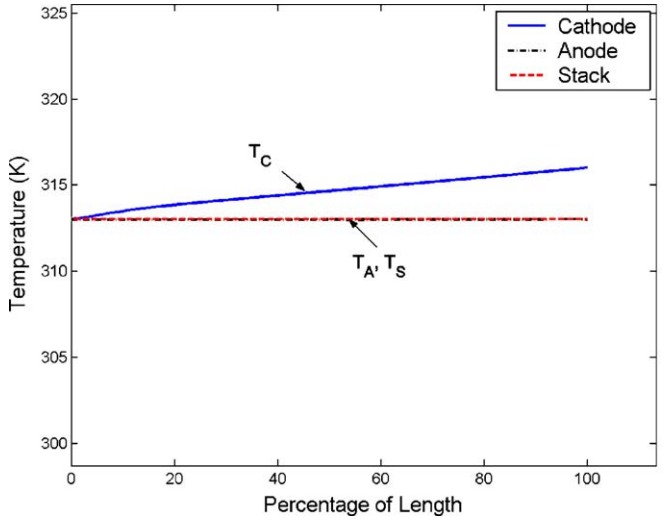

Fig. 26. Flow temperatures and stack temperature distribution along the channel.

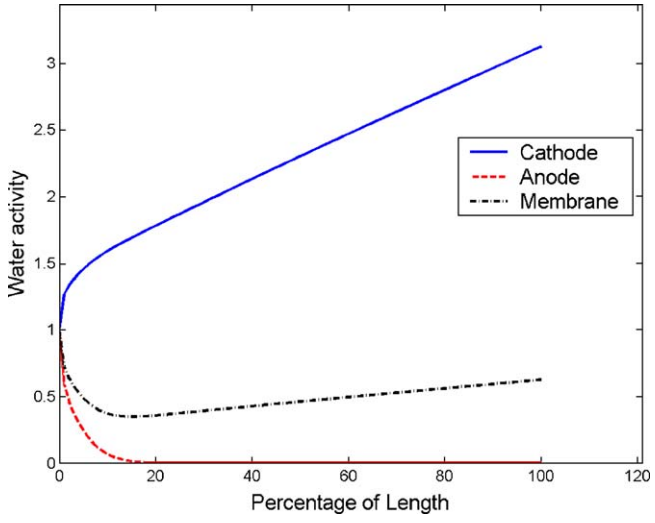

Fig. 28. Water activity distribution along the channel in the base case of constant stack temperature.

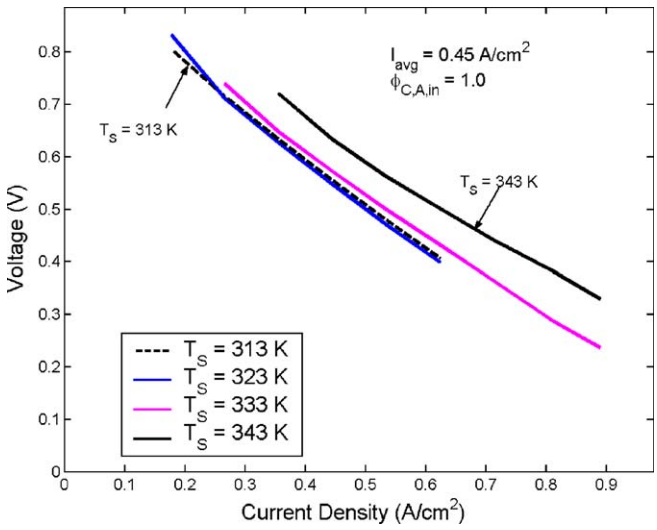

Fig. 29. Polarization curve for different stack temperature.

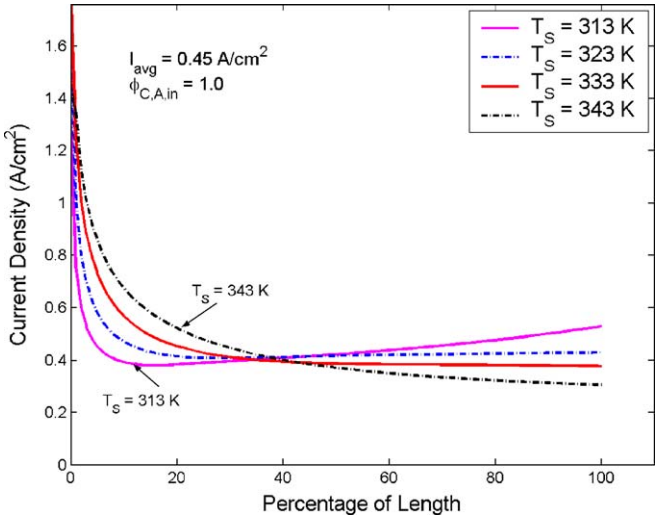

Fig. 30. A comparison of current profiles along the channels with the different inlet stream temperatures.

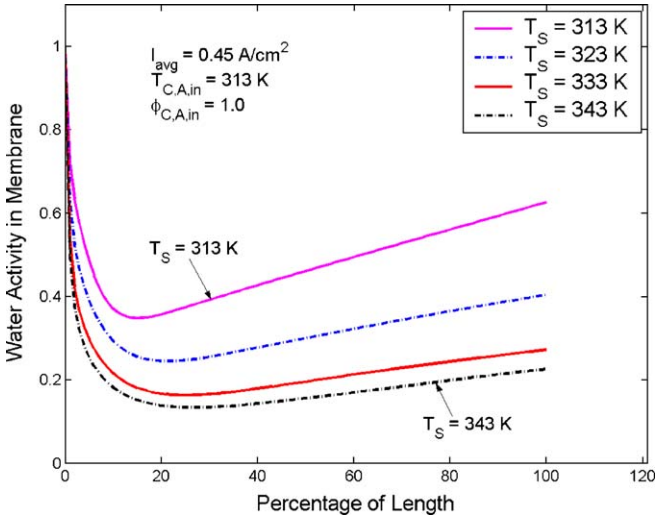

Fig. 31. A comparison of water activity in membrane along the channels with the different inlet stream temperatures.

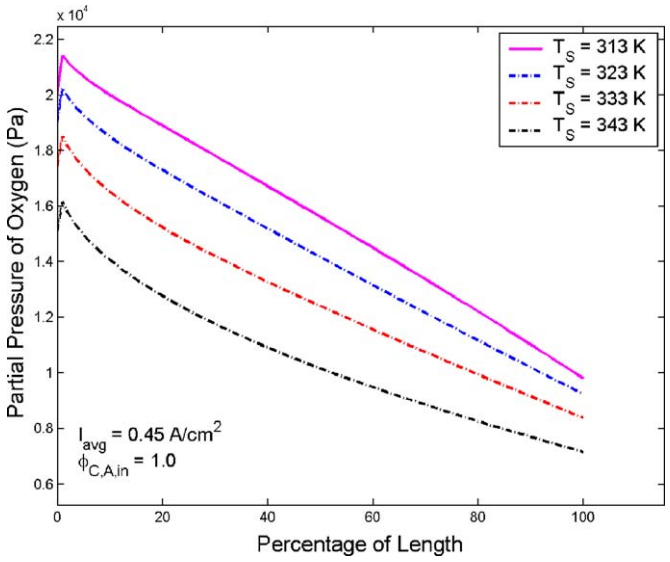

Fig. 32. A comparison of oxygen partial pressure along the channels with the different inlet flow temperatures.

a small amount of oxygen is consumed and the partial pressure of oxygen is high. When the stream moves down the channel, more water is produced and the membrane is hydrated, which increases the water activity as well as the speed of electrochemical reaction. Therefore, the current density increases in the later part of the channel. At high inlet temperature, sufficient water has been carried by the gas at the initial phase and the speed of electrochemical reaction is fast. As a result, more oxygen is consumed and the partial pressure of oxygen decreases quickly. Eventually, these factors lead to reduced electrochemical reaction rates and decrease of the current density throughout the rest of the channel. Since the simulations provide different flow and temperature fields inside the fuel cell channels for the UST and NST, the reaction speed and the amount of water produced are quite different at each point in the channel. Figs. 29 and 17 are the polarization curves for the UST case and NST case, respectively. In Fig. 29, the difference between high temperature curves, such as 333 and 343 K, is more apparent than for the low temperature (313 and 323 K). On the contrary, the low temperature difference is larger than high temperature in Fig. 17. This means, assuming a constant stack temperature not only affects the analysis of flow conditions, but also changes the simulation result of fuel cell performance.

Since a variable stack temperature more likely occurs in a real fuel cell, it makes sense to replace the constant stack temperature assumption with a variable stack temperature. Actually, this was shown in the experimental data. In Fig. 6, the experimental result has been compared with both the UST case and NST case. It is obvious that the NST case provides a better simulation result.

5. Conclusions

In this research, a model for a single PEM fuel cell has been developed. The simulation based on this model can be used to analyze water transport across the membrane, the water phase change effect, the pressure variation along the channel and the

energy balance. It can also be used to predict the characteristics of the flows inside the channel and analyze the factors that affect the fuel cell performance. Based on this study, the following conclusions can be drawn:

1. The NST model is more accurate than the UST model when predicting a single fuel cell performance.
2. The humidification of both anode and cathode sides is a very important factor affecting the performance of a PEM fuel cell.
3. Increasing the flow inlet temperatures is an approach to overcome the water starvation problem. However, if additional equipment is added, the cost of the fuel cell needs to be considered as well.
4. Increasing the flow pressure can improve the fuel cell performance.
5. Proper liquid water injection at the anode channel inlet can be useful in fuel cell performance improvement. An optimal amount of liquid water could be determined by using the simulations based on the model developed in the present study.
6. Decreasing the cooling temperature is helpful in improving the fuel cell performance.

Acknowledgements

This work was supported by NSERC, and AUTO21^{TM}—a Network of Centers of Excellence.

References

[1] M. Kenny, Presentation at the Fuel Cell Vehicle Technology Conference, UC Davis, Davis, CA, 1998.
[2] A. Bauen, D. Hart, Assessment of environmental benefits of transport and stationary fuel cells, J. Power Sources 86 (2000) 482–494.
[3] CARB, Proposed Amendments to the California Zero Emission Vehicle Program Regulations, 2000.
[4] T. Woegerer, Research, design and construction of proton exchange membrane fuel cell, E.S.419-Project Report, The University of Western Ontario, 1998.
[5] T. Fuller, J. Newman, Water and thermal management in solid–polymer–electrolyte fuel cells, J. Electrochem. Soc. 140 (5) (1993) 1218–1225.
[6] T. Nguyen, R. White, A water and heat management model for proton-exchange-membrane fuel cells, J. Electrochem. Soc. 140 (8) (1993) 2178–2186.
[7] J. Yi, T. Nguyen, An along-the channel model for proton exchange membrane fuel cells, J. Electrochem. Soc. 145 (4) (1998) 1149–1159.
[8] R. Mosdale, S. Srinivasan, Analysis and performance of water and thermal management in proton exchange membrane fuel cells, Electrochim. Acta 40 (4) (1995) 413–421.
[9] J. Amphlett, R. Baumert, R. Mann, B. Peppley, P. Roberge, T. Harris, Performance modeling of BALLARD MARK IV solid polymer electrolyte fuel cell I. Mechanistic model development, J. Electrochem. Soc. 142 (1) (1995) 1–8.
[10] J. Amphlett, R. Baumert, R. Mann, B. Peppley, P. Roberge, T. Harris, Performance modeling of Ballard Mark IV solid polymer electrolyte fuel cell II. Empirical model development, J. Electrochem. Soc. 142 (1) (1995) 9–15.
[11] C. Marr, X. Li, An engineering model of proton exchange membrane fuel cell performance, ARI 50 (1998) 190–200.
[12] K. Dannenberg, P. Ekdunge, G. Lindbergh, Mathematical model of the PEMFC, J. Appl. Electrochem. 30 (2000) 1377–1387.
[13] K. Hertwig, L. Martens, R. Karwoth, Mathematical modeling and simulation of polymer electrolyte membrane fuel cells, Fuel Cells 2 (2) (2002) 61–77.
[14] S. Ge, B. Yi, A mathematical model for PEMFC in different flow modes, J. Power Sources 124 (2003) 1–11.
[15] X. Xue, J. Tang, A. Smirnova, R. England, N. Sammes, System level lumped-parameter dynamic modeling of PEM fuel cell, J. Power Sources 133 (2004) 188–204.
[16] B. Zhou, W. Huang, Y. Zong, A. Sobiesiak, Water and pressure effects on a single PEM fuel cell, J. Power Sources 155 (2006) 190–202.
[17] C. Yunus, B. Michael,;1; Thermodynamics—An Engineering Approach, 4th ed., The McGraw-Hill Companies, IBSN: 0-07-238332-1.
[18] M. Lampinen, M. Fomino, Analysis of free energy and entropy changes for half-cell reactions, J. Electrochem. Soc. 140 (12) (1993) 3537–3546.
[19] Handbook of Chemistry and Physics, 62nd ed., CRC Press, Boca Raton, FL, 1981.
[20] NEXAtm Power Module Installation Manual, Ballard Power Systems Inc., 2002.
[21] T. Springer, T. Zawodzinski, S. Gottesfeld, Polymer electrolyte fuel cell model, J. Electrochem. Soc. 138 (8) (1991) 2334–2342.
[22] F. Liu, B. Yi, D. Xing, J. Yu, H. Zhang, Nafion/PTFE composite membranes for fuel cell applications, J. Membr. Sci. 212 (2003) 213–223.